Springer

KSME

Journal of Mechanical Science and Technology 26 (3) (2012) 731~740
www.springerlink.com/content/1738-494x
DOI 10.1007/s12206-011-1233-y

Active vibration control of clamped beams using positive position feedback controllers with moment pair †

Changjoo Shin[1], Chinsuk Hong[2,*] and Weui Bong Jeong[1]

[1]*School of Mechanical Engineering, Pusan National University, Busan, 609-735, Korea*
[2]*School of Mechanical Engineering, Ulsan College, Ulsan, 680-749, Korea*

(Manuscript Received June 29, 2011; Revised September 28, 2011; Accepted November 17, 2011)

Abstract

This paper investigates the active vibration control of clamp beams using positive position feedback (PPF) controllers with a sensor/moment pair actuator. The sensor/moment pair actuator which is the non-collocated configuration leads to instability of the control system when using the direct velocity feedback (DVFB) control. To alleviate the instability problem, a PPF controller is considered in this paper. A parametric study of the control system with PPF controller is first conducted to characterize the effects of the design parameters (gain and damping ratio in this paper) on the stability and performance. The gain of the controller is found to affect only the relative stability. Increasing the damping ratio of the controller slightly improves the stability condition while the performance gets worse. In addition, the higher mode tuned PPF controller affects the system response at the lower modes significantly. Based on the characteristics of PPF controllers, a multi-mode controllable SISO PPF controller is then considered and tuned to different modes (in this case, three lowest modes) numerically and experimentally. The multi-mode PPF controller can be achieved to have a high gain margin. Moreover, it reduces the vibration of the beam significantly. The vibration levels at the tuned modes are reduced by about 11 dB.

Keywords: Active vibration control; Positive position feedback control; Non-collocated system; Open loop transfer function

1. Introduction

Structures should be designed to exclude unintended vibrations, inevitably generated by unwanted disturbances due to various sources. The unwanted disturbances lead to undesired vibration of structures, and the structural vibrations cause weak structural reliability, functional inaccuracy or structural damages. Reduction of the vibration can solve these problems.

Structural vibrations can be reduced by several approaches in two categories: classical methods (structural redesign, and passive control, for example) and active control methods. For classical methods, the passive control method is commonly adapted, because the structural redesign generally leads to high expenses. The passive control methods include damping materials, barriers, decouplers, mass loadings and so on. These passive treatments work more effectively at higher frequencies and so they have practical limitations in reducing low frequency vibrations which are the dominant causes of structural weaknesses and damages. An alternative method for reducing structural vibrations is active vibration control (AVC), which has emerged as a viable technology to low frequency control [1]. Representative active vibration controls are as follows: direct velocity feedback (DVFB) and positive position feedback (PPF).

DVFB is an active vibration control method based on the structural velocity feedback. It is a simple proportional controller. The controller can be just a power amplifier, and so it can be implemented at low cost. In addition, DVFB produces skyhook damping [2], which reduces vibrations at all the frequencies when the actuator generates a point force at the feedback sensor location. This collocated sensor/actuator configuration is described as dual, making DVFB unconditionally stable with an infinite gain margin. Elliott [3] and Balas [4] suggested a robust AVC system using DVFB with a collocated sensor/force actuator pair.

However, DVFB has severe instability problems when the actuator generates a moment pair (by a PZT patch, for example) and the feedback velocity is taken at the mid-point of the moment pair [5]. The instability is caused by the non-collocation of the sensor/moment pair actuator. The non-collocation causes a phase shift due to the geometrical difference between the positions of the sensor and the actuation [6]. Since the phase shift is proportional to the frequency, this source of instability works critically at a high frequency [7].

† This paper was recommended for publication in revised form by Associate Editor Hyoun Jin Kim
* Corresponding author. Tel.: +82 52 279 3134, Fax.: +82 52 279 3137
E-mail address: cshong@uc.ac.kr

Hong implemented DVFB control system with a non-collocated sensor/actuator configuration for aluminum beams analytically and experimentally [8]. They found that the control system becomes only conditionally stable due to the non-collocation, and so the gain margin can hardly be obtained. Eventually, the performance of DVFB control system with non-collocated sensor/actuator configuration is limited. To alleviate the sources of the instability when using a moment pair actuator, Gardonio [9] suggested a phase leg compensator and he applied it for a multi-channel smart panel. They found that the phase compensator improves the stability status. Hong [10] successfully implemented a robust DVFB for honeycomb structures since the honeycomb structure is found to have low pass filter mechanism. The low pass filter mechanism leads to roll-offs at high frequencies so that the control system is stabilized. Hong [11] also suggested a solution to improve stability using triangularly shaped PZT actuators. They placed the triangular PZT actuator at the end of a fixed beam to make a collocated configuration.

In this context, we consider a PPF controller using a moment pair actuator to be an alternative method for solving stability problems due to the non-collocation of the sensor/moment pair actuator. The PPF controller was initially used to suppress the vibration of large flexible structures [12, 13]. It has been then used for many applications [14-16]. It works like a dynamic absorber, which is commonly used to control resonant vibration using a single degree of freedom mechanical system whose resonance is tuned to the structural resonance to be controlled. The PPF controller is also a single degree of freedom system electronically implemented with its resonance frequency tuned to one of the structural resonance frequencies. This control system has hence outstanding advantages. The control system is robust and performs significantly well at the target frequency, because the high control action can be generated at the resonance of the controller due to the tuning stated in literatures [12, 14]. Additionally, the control instability due to the non-collocation of the sensor/actuator can be removed by the low pass filter behavior of the PPF controller leading to rapid roll-offs in the open-loop transfer function at high frequencies [17]. The tuning scheme and the low pass filter behavior of the PPF controller are the main feature for its robustness and good performance.

In this paper, an active control of clamped beams using PPF controller with the sensor/moment pair configuration (non-collocation) is investigated. This study consists of the parametric study of the design parameters of PPF controllers and the implementation of a multi-mode PPF controller designed based on the parametric study. In section 2, the equation of motion of a clamped beam with the lumped masses for sensors/actuators is formulated. In section 3, the proposed PPF control system is mathematically formulated and then derived for a multi-mode controllable SISO system implementation. Section 4 examines how the design parameters of the PPF controllers affect the stability and performance of the PPF controllers. In section 5, simulations of the stability and performance of the multi-mode controllable SISO PPF control system for the clamped-clamped beams are conducted. Experiments on the PPF controller are presented in section 6. Finally, in section 7, conclusions are given.

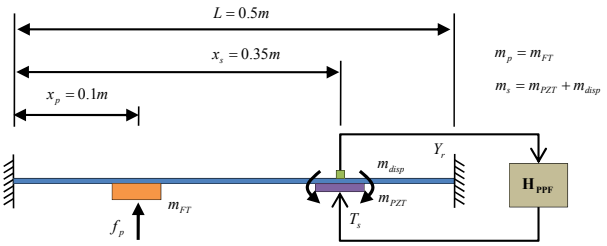

Fig. 1. Simulation model for active feedback control system for a clamped beam with a sensor/actuator pair system.

2. Equation of motion of clamped beams with lumped masses of sensors and actuators

Consider a clamped-clamped beam having lumped masses as shown in Fig. 1. The lumped masses represent the force transducer, the PZT actuator, and the displacement sensor. The equation of motion for the system can be obtained as [18]

$$EI(1+j\eta)\frac{\partial^4 y}{\partial x^4}+\rho A\frac{\partial^4 y}{\partial t^4}+\left(m_p\frac{\partial^2 y}{\partial t^2}\delta(x-x_p)+m_s\frac{\partial^2 y}{\partial t^2}\delta(x-x_s)\right)$$
$$=f_p\delta(x-x_p)+\frac{\partial}{\partial x}T_s\left[\delta(x-x_{s2})-\delta(x-x_{s1})\right] \quad (1)$$

where E is Young's modulus, I is the moment of inertia of the beam and η is the loss factor to be expressed as the equivalent viscous damping, $2\zeta_{sn}$. ρ is the mass density, A is the cross sectional area, m_p is the mass of the force transducer on the beam, and m_s is the total mass of the piezoceramic patch and the displacement sensor on the beam. So $m_p = m_{FT}$ and $m_s = m_{PZT} + m_{disp}$. f_p is the external force applied at x_p and T_s is the control moment pair at x_{s1} and x_{s2}. For harmonic motions, the response, y, can be expressed as

$$y(x,t) = Y(x,\omega)e^{j\omega t}. \quad (2)$$

Assuming that the general solution is expressed as a superposition of the modal function,

$$Y(x,\omega) = \mathbf{\Phi}(x)\mathbf{p}(\omega) \quad (3)$$

where $\mathbf{p}$ is the column vector of modal displacement, $\mathbf{\Phi}(x)$ is the row vector of the mode shape function at the location of x, defined by

$$\mathbf{p}(\omega) = \left[p_1(\omega) \quad p_2(\omega) \quad \cdots \quad p_N(\omega)\right]^T, \text{ and} \quad (4)$$
$$\mathbf{\Phi}(x) = \left[\phi_1(x) \quad \phi_2(x) \quad \cdots \quad \phi_N(x)\right]. \quad (5)$$

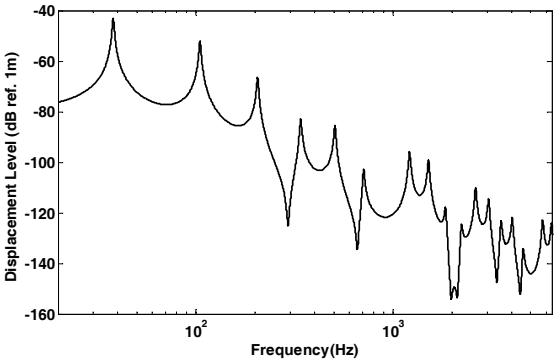

Fig. 2. Displacement of the clamped beam at the feedback sensor location ($x_s = 0.7L$), which is excited by a unit force at $0.2L$.

Utilizing the orthogonality of the mode shape functions leads to the matrix equation as

$$\left[-\omega^2\mathbf{I} + j\mathbf{diag}(2\zeta_{sn}\omega_{sn}\omega) + \mathbf{diag}(\omega_{sn}^2)\right]\mathbf{p} = \mathbf{\Phi}(x_p)^T f_p + \left[\frac{\partial\mathbf{\Phi}(x_{s1})}{\partial x} - \frac{\partial\mathbf{\Phi}(x_{s2})}{\partial x}\right]^T T_s \tag{6}$$

where ζ_{sn} is the nth modal damping ratio, ω_{sn} is the nth frequency of the structure, and $\frac{\partial\mathbf{\Phi}(x)}{\partial x}$ is the row vector of differentiation of the mode shape function at the location of x , defined by

$$\frac{\partial\mathbf{\Phi}(x)}{\partial x} = \left[\frac{\partial\phi_1(x)}{\partial x} \quad \frac{\partial\phi_2(x)}{\partial x} \quad \cdots \quad \frac{\partial\phi_N(x)}{\partial x}\right]. \tag{7}$$

The response at the sensor point ($x = x_s$) of the clamped beam subjected to an external force and moments can be obtained as

$$Y(x_s,\omega) = \mathbf{\Phi}(x_s)\mathbf{p}(\omega). \tag{8}$$

Fig. 2 shows the displacement of the clamped beam at $0.7L$, excited by the primary force ($f_p = 1$) at $x_s = 0.2L$ without control. Note that, however, the lumped masses at $0.2L$, for the mass of the upper part of the force transducer, and at $0.7L$, for the masses of the displacement sensor and the PZT actuator, are taken into account. The mechanical properties and masses used in this simulation are listed in Table 1.

The dominant vibrations occur at the lowest three modes. These vibration levels are -38.06, -52.06, and -66.65 (dB ref. 1m), respectively. In this study, these modes are selected as the target modes to be controlled.

3. Positive position feedback control

The PPF controller was initially proposed by Fanson and Caughy [12]. They successfully implemented on active vibration control system for large structures using a sensor and actuator pair. The PPF controller was developed to control for one mode of the control system. They expressed the equations of PPF control as a pair of 1 DOF structure and compensator on the modal domain. The compensator generates the control force which acts as a damping force at target mode of the structure to be controlled. Note that the equations are defined on the modal domain. On the other hand, the system lies on the physical domain. Hence, the behaviors of both structure and compensator should express on the physical domain. The behavior of the structure is already expressed as Eqs. (6) and (8). In addition, the compensator equation for PPF control is as follows:

$$\ddot{q}_i + 2\zeta_{ci}\omega_{ci}\dot{q}_i + \omega_{ci}^2 q_i = g_i\omega_{si}^2\omega_{ci}^2 p_i \quad i = 1,2,\cdots,N_c \tag{9}$$

where q_i is the ith response of the compensator, ζ_{ci} and ω_{ci} are the ith damping ratio and the ith natural frequency of the compensator, respectively. g_i is the ith feedback gain, ω_{si} is the ith natural frequency of the structure to be controlled, and N_c is the number of the compensators.

Table 1. Mechanical properties.

Young's modulus (GPa)	E	78
Density (kg/m^3)	ρ	2850
Length (m)	L	0.5
Width (m)	b	0.03
Thickness (m)	h	0.002
Loss factor	η	0.002
Mass of upper part of force transducer (kg)	m_{FT}	0.006
Mass of PZT (kg)	m_{PZT}	0.009
Mass of displacement sensor (kg)	m_{disp}	0.0024

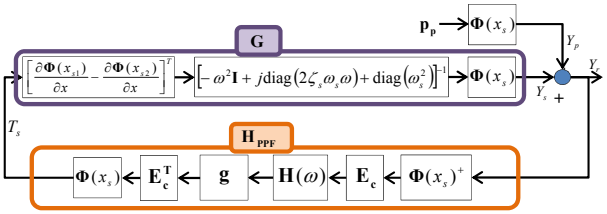

Fig. 3. Block diagram of active feedback control using PPF controller.

Fig. 3 shows the block diagram of the active control system using PPF controller for the clamped beam shown in Fig. 1. It should be noted that the feedback sensor mounted on the beam measures the physical displacement, while the compensator denoted by Eq. (9) requires the modal displacement. The modal displacement can be approximately evaluated from the measured displacement by using Eq. (8). Pre-multiplying the pseudo inverse of the mode shape matrix at $x = x_s$, the modal displacement can be expressed as

$$\mathbf{p} = \mathbf{\Phi}(x_s)^+ Y_r \tag{10}$$

where $^{+}$ denotes the pseudo inverse. It should be also noted that the moment pair actuator generates control action, T_s, in physical domain, while the compensator is ready to supply the signal, q_i, for each mode to the compensator. The magnitude of the control action (which is in practice a voltage signal driving the moment pair actuator, PZT patch for example) is composed by the superposition:

$$T_s = \mathbf{\Phi}(x_s)\mathbf{E_c}^T\mathbf{q} \tag{11}$$

where $\mathbf{E_c}$ represents the transform matrix to extract the control modes from the modal displacement.

Now, we can define the plant response which is the feedback sensor signal to the unit control action, $T_s = 1$. From Eqs. (6) and (8),

$$G(\omega) = \mathbf{\Phi}(x_s)\left[-\omega^2\mathbf{I} + j\mathbf{diag}(2\zeta_s\omega_s\omega) + \mathbf{diag}(\omega_s^2)\right]^{-1} \times\left[\frac{\partial\mathbf{\Phi}(x_{s1})}{\partial x} - \frac{\partial\mathbf{\Phi}(x_{s2})}{\partial x}\right]^T . \tag{12}$$

We can also define the transfer function of the compensator, $\mathbf{H_{PPF}}(\omega)$, which is the output signal, T_s, from the compensator to the sensor signal, Y_r:

$$\mathbf{H_{PPF}}(\omega) = \mathbf{\Phi}(x_s)\mathbf{E_c}^T\mathbf{gH}(\omega)\mathbf{E_c}\mathbf{\Phi}(x_s)^+ \tag{13}$$

where

$$\mathbf{g} = \mathbf{diag}(g_i\omega_{si}^2) \text{, and} \tag{14}$$

$$\mathbf{H}(\omega) = \mathbf{diag}\left(\frac{\omega_{ci}^2}{\omega_{ci}^2 - \omega^2 + j2\zeta_{ci}\omega_{ci}\omega}\right). \tag{15}$$

The open loop transfer function (OLTF) can be finally obtained by considering the relationship of the signals (Y_r, Y_p and Y_s shown in Fig. 3),

$$\begin{aligned} Y_r(\omega) &= Y_p(\omega) + Y_s(\omega) \\ &= \mathbf{\Phi}(x_s)\mathbf{p_p}(\omega) + \mathbf{G}(\omega)T_s(\omega) \end{aligned} \tag{16}$$

where $\mathbf{p_p}$ is the modal displacement by external force. Using Eqs. (11) and (16), the controlled displacement at the sensor can be

$$Y_r(\omega) = \left[\mathbf{I} + (-\mathbf{GH_{PPF}})\right]^{-1}\mathbf{\Phi}(x_s)\mathbf{p_p}(\omega) . \tag{17}$$

Reminding the standard form of the closed loop transfer function of negative feedback control systems, the OLTF can be written from Eq. (17) as,

$$\mathbf{OLTF}(\omega) = -\mathbf{GH_{PPF}} . \tag{18}$$

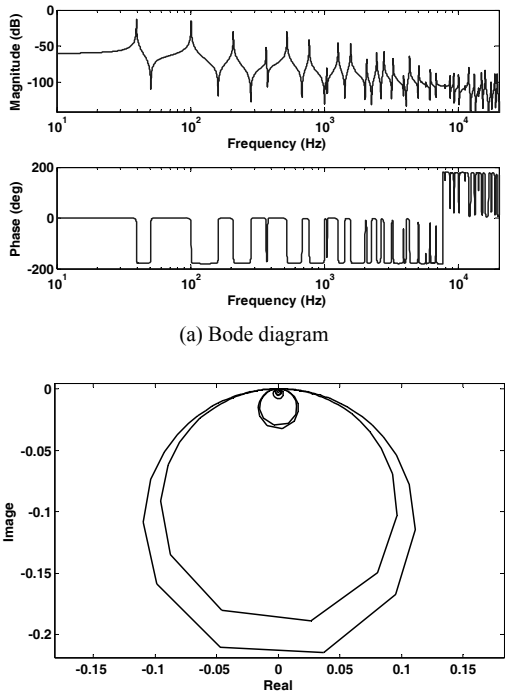

(a) Bode diagram

(b) Nyquist diagram

Fig. 4. Plant response at $0.7L$.

Fig. 4 shows the plant response when $x_s = 0.7L$. The phase lies between -180° and 0° up to 7.7kHz while it lies between 0° and 180° at frequencies higher than 7.7kHz, as shown in Fig. 4(a). This phase shift occurs where the wave length of the mode is shorter than the half length of the PZT in high frequencies [19]. Fig. 4(b) shows that the plant cannot obtain the active damping without aids of controllers. Note that the location of the sensor/actuator at $x_s = 0.7L$ is taken from previous work done by Hong [19]. He studied the effected of the location of the sensor/actuator pair on the stability and the performance of control systems. He revealed that the system is under conditionally stable and has little gain margin when the sensor/actuator pair is located at the ends of the structure. In order to ensure the stability of the feedback system, the moment pair actuator should be located between $0.3L$ and $0.7L$. So, the location of the sensor/actuator pair is selected at $x_s = 0.7L$ in order to maintain a high gain margin.

Fig. 5 shows the transfer function of the PPF controller. This controller is tuned to the third mode resonance of the structure (208 Hz in this case). The controller is specially designed to produce the active damping at the tuned mode with a high gain margin. This can be achieved by the two features: phase shift and high frequency roll-off. The phase shift is occurred at the tuned mode from 0° to -180° as shown in Fig. 5. It helps to give the active damping to the control system. The transfer function of the PPF controller, shown in Fig. 5, gives a high amplification at the tuned mode and gives a roll-off over the high frequencies. Therefore, it can reduce unknown effects of unmodeled response in the high frequency

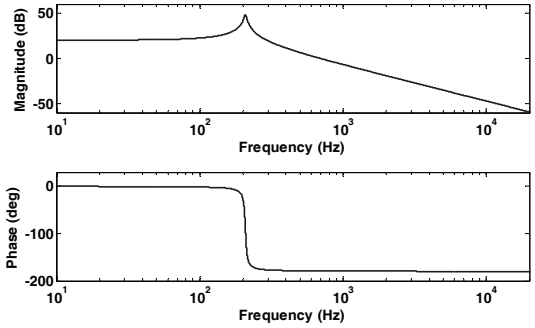

Fig. 5. Bode diagram of the response of the third mode tuned PPF controller.

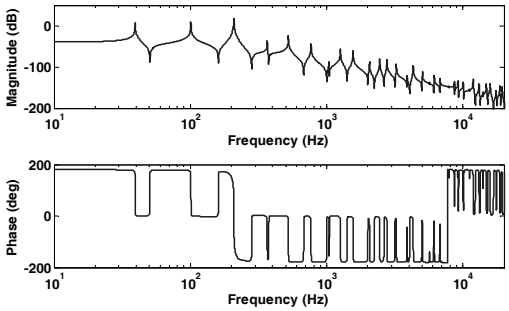

(a) Bode diagram

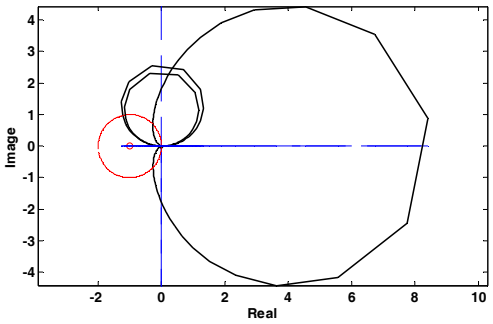

(b) Nyquist diagram

Fig. 6. Open loop transfer function with a PPF controller tuned to the third mode of the structure.

range.

Fig. 6 shows the OLTF of the active control system with the PPF controller tuned to the third mode of the structure. The magnitude of the OLTF is amplified at the tuned mode and the corresponding phase is shifted by $180°$, as shown in Fig. 6(a). This phase shift causes the Nyquist curve of this mode to be in the right half plane, as shown in Fig. 6(b). Note that the phase shift is due to the phase characteristics of the PPF controller shown in Fig. 5. It can be also seen that the magnitude of the OLTF is decreased as the frequency is increased at the frequencies higher than the tuning frequency. This high frequency roll-off is also due to the magnitude characteristic of the PPF controller. The high frequency roll-off of the PPF controller is similar to that of the second order low pass filter. Since potential instability due to the non-collocated sensor/actuator pair can be alleviated by the high frequency roll-offs, a high gain margin of the control system can be obtained.

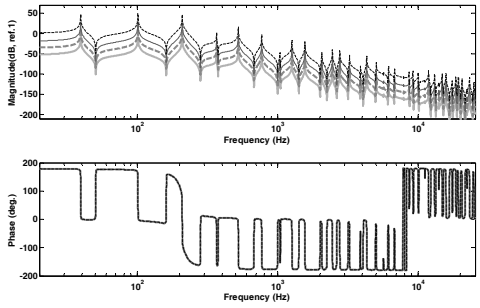

(a) Bode diagram

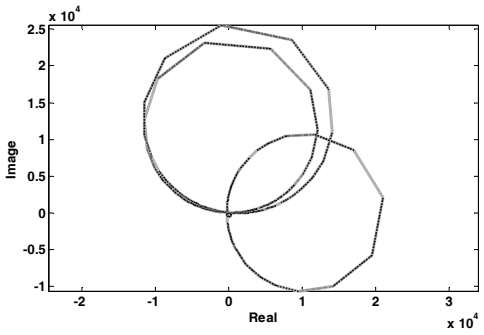

(b) Nyquist diagram

Fig. 7. Variation of the open loop transfer function of active control systems at $0.7L$ with the feedback gain of PPF controllers with a sensor/actuator pair. The PPF controllers are tuned to the third mode with damping ratio of 8.0×10^{-2} and gains of 2.2×10^{-4} (thick solid line), 1.5×10^{-3} (thick dashed line), 1.0×10^{-2} (faint solid line) and 1.0×10^{-1} (faint dashed line).

4. Effects of design parameters of PPF controllers

The design parameters of the PPF controller are the tuning frequency, the damping ratio and the feedback gain. They significantly affect the stability and the performance of the control system. The tuning frequency is the resonance frequency of the PPF controller which is selected to be a resonance frequency of the structure to be controlled [20]. In this section, therefore, the effects of the gain and the damping ratio of the PPF controller on the stability and the performance of the control system are mainly investigated.

Fig. 7 shows the variation of the OLTF of the third mode tuned PPF controller for the gains of 2.2×10^{-4} (thick solid line), 1.5×10^{-3} (thick dashed line), 1.0×10^{-2} (faint solid line) and 1.0×10^{-1} (faint dashed line). The damping ratio of the PPF controller is set to 8.0×10^{-2}. The magnitude of the OLTF is increased at all the frequencies as the gain is increased, as shown in Fig. 7(a), while the phase of the OLTF is not changed. Fig. 7(b) shows the OLTF normalized by the corresponding feedback gains for the four gains. The four Nyquist curves are perfectly overlapped owing to the gain normalization. This overlap indicates that the magnitude of the OLTF is proportional to the gain so that the active damping at

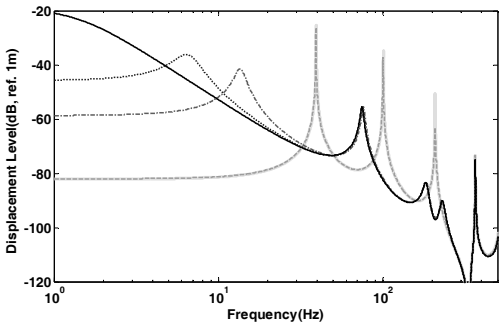

Fig. 8. Variation of the performance of active control systems at $0.7L$ with the feedback gains of PPF controllers with a sensor/actuator pair under the fixed damping ratio of 8.0×10^{-2}. The PPF controllers are tuned to the third mode with gains of 7.0×10^{-4} (dashed line), 8.8×10^{-3} (dash-dotted line), 9.5×10^{-2} (dotted line) and 9.73×10^{-2} (thin solid line). And uncontrolled response is faint solid line for comparison with controlled response.

the tuned mode increases as the gain increases. There are the two Nyquist curves in the first and second quadrants. These two responses correspond to the modes lower than the tuned mode. This behavior is due to the low pass filter effect of the PPF controller, as shown in Fig. 5. This effect leads to the enhancement in the close loop response where the Nyquist curves of the two modes are in the unit circle about $(-1, j0)$ at some frequencies.

Fig. 8 shows the variation of the displacement response of the closed loop control system at $0.7L$ of the beam with feedback gains of 7.0×10^{-4} (dashed line), 8.8×10^{-3} (dot-dashed line), 9.5×10^{-2} (dotted line) and 9.73×10^{-2} (thin solid line) subjected to a PPF controller tuned to the third mode of the structure. The uncontrolled displacement response (fain solid line) to the disturbance, f_p, at $0.2L$ is also shown in Fig. 8 for comparison. The damping ratio of 8.0×10^{-2} is used. Two key features are shown. First, the closed loop displacement at the feedback sensor ($x_s = 0.7L$) is decreased at the target mode as the gain is increased. This is illustrated by the increase of the magnitude of the OLTF as the gain is increased, shown in Fig. 7(a). Second, new peaks around the tuning frequency are also found. The difference between the frequencies of the new peaks increases as the gain is increased, as if the mass ratio is increased in dynamic absorbers [21].

In addition to the effects of the gain on the response of the closed loop control system around the tuning frequency, the gain also affects the response at the modes lower than the tuning frequency: significant changes in magnitude and resonance frequencies. For the gain of 8.8×10^{-3}, the resonance frequencies of the first and the second modes are significantly decreased: the frequency of the first mode decreased from 39Hz to 14Hz and that of the second mode from 101Hz to 85Hz, with magnitude reduction of 45dB at the tuned mode. In the case of the gain slightly increased to 9.5×10^{-2}, the first resonance frequency is decreased further while the second resonance remains. A further increase of the gain makes the

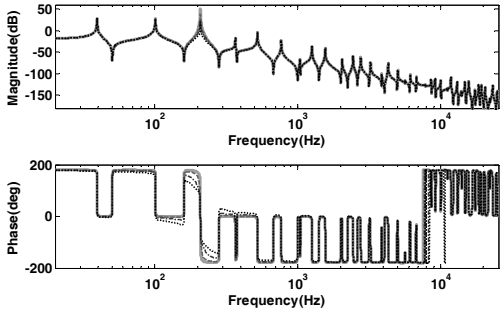

(a) Bode diagram

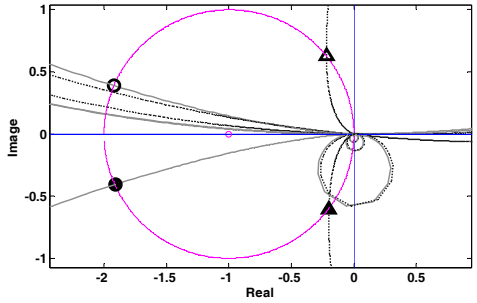

(b) Zoomed Nyquist diagram

Fig. 9. Variation of the open loop transfer function of active control systems at $0.7L$ with the damping ratio of PPF controllers with a sensor/actuator pair. The PPF controllers are tuned to the third mode with the gain of 5.0×10^{-2} and damping ratio of 5.0×10^{-3} (solid line), 2.0×10^{-2} (dashed line), 8.0×10^{-2} (dash-dotted line) and 2.0×10^{-1} (dotted line).

first resonance approach to 0 Hz. This phenomenon can be explained by the response of the OLTF crossing the negative real axis around 0 Hz in the Nyquist plot. These responses are also within the unit circle about the $(-1, j0)$ point.

The Nyquist curves at the lower modes move toward the Nyquist point and vary the frequency contents inside the unit circle. This behavior at the end leads to the variation of the lower mode response in terms of the magnitude and the natural frequency.

The variation of the resonance frequency at the lower modes can also be illustrated by the behavior of the transfer function of the PPF controller shown in Fig. 5. The essential feature of the transfer function of the PPF controller for this explanation is the phase behavior, in that there is no phase change at frequencies lower than the target frequency. Since the feedback signal is proportional to the displacement at the actuator location, the PPF controller plays a role of the stiffness at frequencies lower than the target frequency. Note that the PPF controller decreases the stiffness as the gain increases when connected positively as shown in Fig. 1. Due to the phase change of $90°$ at the target frequency, the PPF controller generates a damping force. Moreover, owing to the phase change of $180°$ at frequencies higher than the target frequency, the PPF controller generates an inertia force.

Fig. 9 shows the variation of the OLTF of the third mode

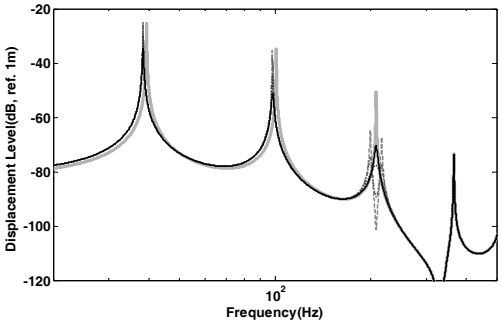

(a) Controlled responses

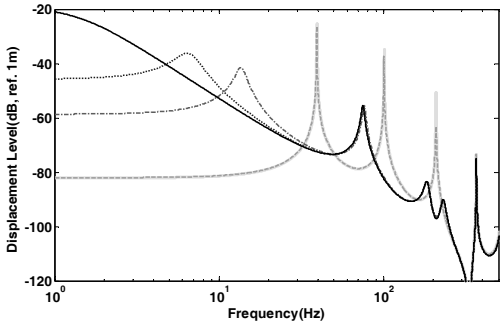

(b) Controlled responses at the third mode

Fig. 10. Variation of the performance of active control systems at $0.7L$ with the feedback damping ratios of PPF controllers with a sensor/actuator pair under the fixed gain of 1.0×10^{-2}. The PPF controllers are tuned to the third mode with damping ratios of 5.0×10^{-3} (dashed line), 2.0×10^{-2} (dash-dotted line), 8.0×10^{-2} (dotted line) and 2.0×10^{-1} (thin solid line). And uncontrolled response is faint solid line for comparison with controlled response.

tuned PPF controller with the damping ratios of 5.0×10^{-3}, 2.0×10^{-2}, 8.0×10^{-2} and 2.0×10^{-1}. The gain of 5.0×10^{-2} is used for this simulation. As shown in Fig. 9(a), the magnitude of the OLTF is decreased as the damping ratio is increased at the tuned mode, but it is not changed at the other modes. The phase around the tuned mode is significantly changed when the damping ratio is increased. The phases of the OLTF are varied in a wider frequency range as increasing damping ratio, as shown in Fig. 9(a). This phase behavior can be represented more clearly as shown in Fig. 9(b). The two hollow marks (○ and △) are all at 202 Hz : ○ for ζ_c = 5.0×10^{-3} and △ for ζ_c = 2.0×10^{-1}. Besides, the two solid marks (● and ▲) are all at 215 Hz. : ● for ζ_c = 5.0×10^{-3} and ▲ for ζ_c = 2.0×10^{-1}. The bandwidth of the PPF controller is not varied with the change of the damping ratio. Also the responses within the unit circle about $(-1, j0)$ move away from the Nyquist point as the damping ratio increases. So, the control system is stabilized with the increase of the damping.

Fig. 10 shows the variation of the closed loop displacement response with the damping ratio of the PPF controller. The PPF controller is tuned to the third mode of the structure. The damping ratios of the PPF controllers are 5.0×10^{-3}, 2.0×10^{-2}, 8.0×10^{-2} and 2.0×10^{-1} for this simulation. The feedback gain of the PPF controller is set to 1.0×10^{-2}.

The control performance (reduction in the structural response) is decreased as the damping ratio of the PPF controller is increased, as we expected from the examination of the OLTF shown in Fig. 9(a). Note that new peaks at both side of the tuning frequency are emerged, and their levels are decreased as the damping ratio is increased. This is explained by the enhancement directly related to the existence of the OLTF response in the unit circle about $(-1, j0)$. There exist two frequencies (202 Hz and 215 Hz in this case) in the spectrum of the closed loop displacement where the displacement levels do not vary as the damping ratio change. These two frequencies correspond to the points where the Nyquist curves cross the unit circle, as shown in Fig. 9(b). The effective bandwidth of the PPF controller is not, therefore, changed. But the responses of the first and second modes are shifted to the lower frequency range by about 2 Hz. This shift is due to the reduction of the structural stiffness by the PPF controller [20].

5. Implementation and evaluation of the multi-mode PPF controller

Based on the examination of the behavior of the PPF controller, a SISO multi-mode control is examined in this section. To realize the SISO multi-mode PPF controller, a control signal is obtained by summation of the signals from PPF controllers which are tuned to each mode and connected in parallel form. The parameters of the PPF controllers are set based on the results of the parametric study conducted in the previous section. The controllers are designed from the highest mode first and then to the lower modes in order to adapt the effects of the higher mode controller on the response of the lower modes.

Fig. 11 shows the OLTF of the active PPF control system with the sensor/moment pair actuator at $0.7L$ of the clamped-clamped beam. The first mode tuned controller was designed for gain of 2.8×10^{-2} and damping ratio of 5.0×10^{-2}. The second mode tuned controller was designed for gain of 1.4×10^{-3} and damping ratio of 5.0×10^{-2}. The third mode tuned controller was designed for gain of 7.7×10^{-3} and damping ratio of 5.0×10^{-2}. It can be seen from Fig. 11(a) that the magnitudes of the first, second and third modes of the combined OLTF are quite high. The performances at these three modes are almost the same as those of the single mode tuned PPF controller at the tuned modes. The phase is almost in the active damping region of $\pm90°$ at the tuned modes. Hence, the structural displacement can be reduced at the first, second and third modes. As shown in Fig. 11(b), the multi-mode controller is stable with a high gain margin according to OLTF. The magnitude of the OLTF response within the unit circle about the $(-1, j0)$ point is smaller than that outside the unit circle. Therefore, the magnitude enhancement is smaller than the reduction around the tuning frequency.

Fig. 12 shows the closed loop response of the clamped

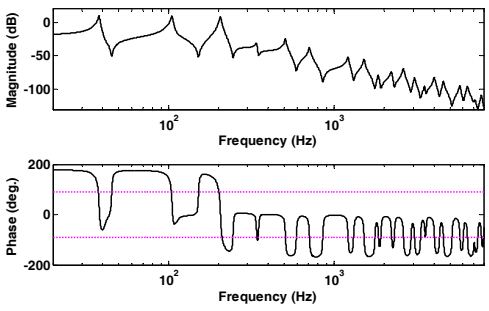

(a) Bode diagram

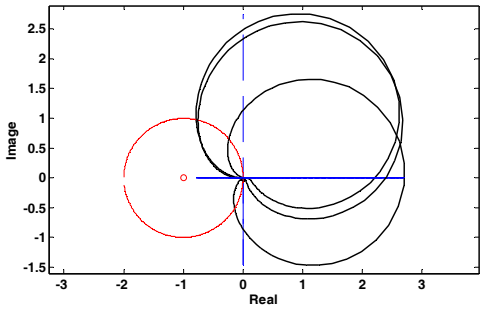

(b) Nyquist diagram

Fig. 11. Final controller open loop transfer function of the sensor/moment actuator pair at $0.7L$ of the clamped-clamped beam.

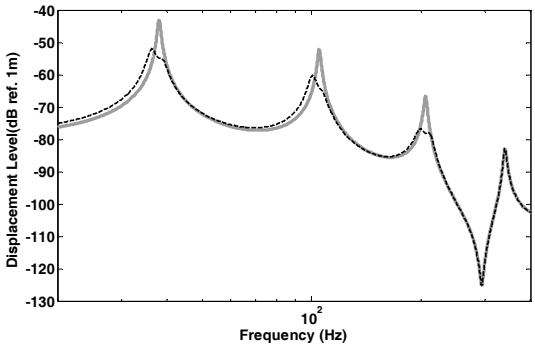

Fig. 12. Displacement of the clamped-clamped beam at $0.7L$, excited by concentrated force at $0.2L$ and subjected to control moment pair at $0.7L$ - without control (solid line) and with control (dashed line).

beam at $0.7L$, excited by a concentrated force at $0.2L$ (solid) and subjected to the control moment pair at $0.7L$ (dashed). The disturbances are reduced about 11dB at each tuned mode, as shown in Fig. 11.

6. Experimental implementation of the PPF controller

Based on the analytic examination of the PPF controller behavior, its performance is experimentally verified for the multi-mode (the first, second and third modes) in this section.

Fig. 13 shows the schematic diagram for the measurement of the PPF control of a clamped beam. An aluminum beam with a length of $0.5m$ is fixed at both ends. A force transducer, B&K 8200, and an exciter, B&K 4810, are located at

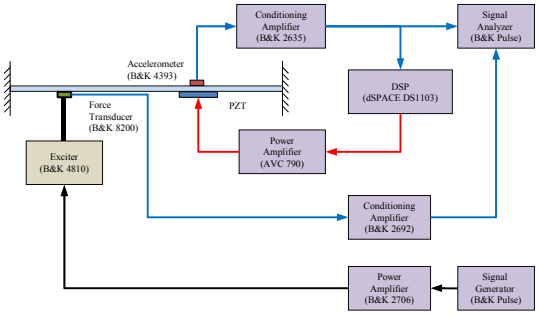

Fig. 13. Schematic diagram for the measurement of the PPF control of a clamped beam.

$0.2L$. An accelerometer, B&K 4393, and a piezoceramic actuator are attached to the beam at $0.7L$. The piezoceramic actuator is a rectangular shaped 1-3 mode PZT patch ($25mm \times 25mm \times 1\mathbf{T}$) whose material properties hold with PZT4 series, manufactured by Kyungwon Ferrite Ind. Co., Ltd (South Korea). The primary disturbance field of vibration is generated by a mini-shaker, B&K 4810, at $x_p = 0.2L$ with a power amplifier, B&K 2706. A signal generator, a built-in module of B&K Pulse, is connected to the power amplifier. A random signal is used in this experiment for the primary disturbance. A force transducer, B&K 8200, is installed between the mini-shaker and the beam to measure the primary force. The measured primary force is used for normalizing the primary field of vibration. To do this, the force transducer is connected to a conditioning amplifier, B&K 2692, and then to the input channel of the signal analyzer, B&K Pulse. The disturbances are measured by the accelerometer, B&K 4393, at $x_s = 0.7L$. The signal from the acceleration is conditioned and double integrated to the displacement signal by using a conditioning amplifier, B&K 2635, and this displacement signal is fed back to the DSP, dSPACE DS1103. The DSP generates a control signal that is input to the power amplifier, PCB AVC 790, to drive the PZT patch control actuator. The DSP is programmed to work as the PPF controller. This practical PPF controller is implemented by programming the transfer

$$\mathbf{H}(\omega) = \mathbf{diag}\left(\frac{\omega_{ci}^2}{s^2 + 2\zeta_{ci}\omega_{ci}s + \omega_{ci}^2} \right) \tag{19}$$

which is a rewritten form of Eq. (15) in the s-domain. Eq. (19) is coded using Matlab/Simulink. The transfer function, Eq. (19), is downloaded to the Rom of the DSP (dSPACE DS1103). Then the DSP works as the PPF controller. To control disturbances of the first, second and third modes, the control signal is obtained by the summation of the signals from each PPF controller, which is tuned to each mode and connected parallel.

Fig. 14 shows the measured open loop transfer function of the multiple mode tuned PPF controller which is tuned to the structural first, second and third modes using a sensor/moment

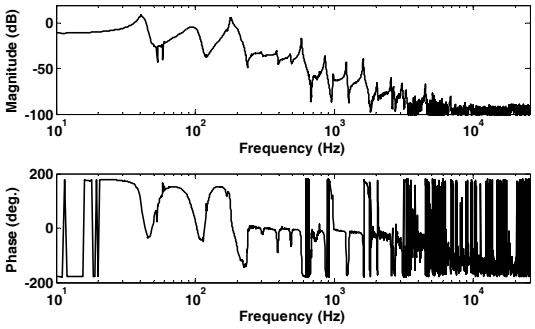

(a) Bode diagram

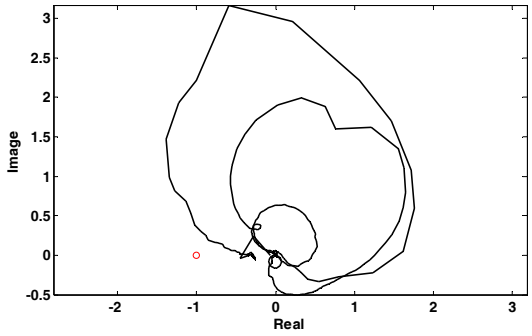

(b) Nyquist diagram

Fig. 14. Measured open loop transfer function of the multiple mode tuned PPF control system tuned to the structural first, second and third modes using a sensor/moment actuator pair for the clamped beam at $0.7L$.

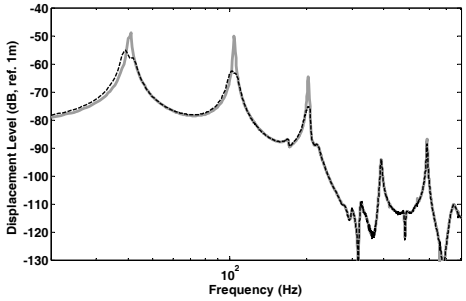

Fig. 15. Measured displacement response of the clamped beam excited by a concentrated force at $0.2L$ (solid line), and when subjected to PPF controller with sensor/moment pair actuator system at $0.7L$ (dashed line).

actuator pair for the clamped beam at $0.7L$. The first mode tuned controller was designed having the gain of 2.5×10^{-2} and the damping ratio of 5.0×10^{-2} . The second mode tuned controller was designed having the gain of 2.5×10^{-2} and the damping ratio of 5.0×10^{-2} . The third mode tuned controller was designed with the gain of 1.5×10^{-3} and the damping ratio of 5.0×10^{-2} . As shown in Fig. 14(a), the magnitude of the tuned modes is 10 dB higher than that of the any other modes, so that we can see the roll-off property of the PPF controller clearly. Therefore, we can expect the high performance at the tuned modes and the unknown effects of the control system will be reduced in the high frequencies. Also, the phase of the tuned modes lies in the active damping region of $\pm90^\circ$. Hence, the structural displacement will be reduced at the first, second and third modes owing to the active damping force. And the response of the open loop transfer function does not cross the $(-1, j0)$ point, so that this control system will be stable, as shown in Fig. 14(b).

Fig. 15 shows the measured displacement response of the clamped beam excited by a concentrated force at $0.2L$ (solid line), and when subjected to PPF controller with sensor/moment pair actuator system at $0.7L$ (dashed line). The structural response is experimentally reduced to about 11dB.

7. Conclusions

This paper investigated the active vibration control of clamp-clamped beams using PPF controllers with non-collocated sensor/moment pair actuator configuration to overcome the instability of DVFB controller due to the phase shift at high frequencies. The moment pair actuator is used as the control actuator and the displacement sensor is used as the feedback sensor located at the opposite center of the moment pair. This non-collocated configuration is the main source of instability problems in control systems. In order to overcome the instability problem due to the non-collocated sensor/moment pair actuator configuration, a SISO system with multiple PPF controllers is implemented based on the results of the parametric study for the design parameters. Following conclusions are highlighted;

A parametric study on the design parameters of the PPF controller was conducted to characterize their effects on the stability and the performance of the controller. The considered design parameters are the gain, and damping ratio of the controller. The magnitude of the OLTF was increased without variation of the phase as the gain was increased. The gain did not thus change the stability characteristics, but did change the performance of the closed loop control system. Furthermore, the difference between the two frequencies at the new peaks due to the PPF controller was increased as the gain was increased. Hence, the gain widened the bandwidth of the reduction at the tuned mode. The magnitude of the OLTF was decreased at the tuned frequency, and the phase of the OLTF was affected in a wider range of the tuned mode as the damping ratio was increased. Increasing the damping ratio made the control system more stable, but the control system required a higher gain to obtain the same performance. Note that the difference between the two frequencies at the new peaks due to the PPF controller did not vary as the damping ratio increased. Finally, when the PPF controller was tuned to a higher mode, the PPF controller significantly affected the response at the lower modes. The natural frequency of the combined system (structure and PPF controller) was decreased at the lower modes since the PPF controller reduced the stiffness.

A multi-mode (the first, second and third modes) controllable PPF controller was implemented and verified to be stable

and of high performance. The control signal was obtained by summation of the signals from each PPF controller, which was tuned to each mode and connected in parallel. The vibration levels at the tuned modes were reduced by about 11dB, as determined numerically and experimentally.

Acknowledgement

This work was partly supported by the 2010 Research Fund of Ulsan College.

References

[1] S. O. R. Moheimani, D. Halim and A. J. Fleming, *Spatial control of vibration theory and experiments*, World Scientific (2003).

[2] M. Serrand and S. J. Elliott, Multichannel feedback control for the isolation of base-excited vibration, *Journal of Sound and Vibration*, 234 (4) (2000) 681-704.

[3] S. J. Elliott, P. Gardonio, T. C. Sors and M. J. Brennan, Active vibroacoustic control with multiple local feedback loops, *Journal of the Acoustical Society of America*, 111 (2) (2002) 908-915.

[4] M. J. Balas, Direct velocity feedback control of large space structures, *Journal of Guidance and Control*, 2 (1979) 252-253.

[5] R. H. Canon and D. F. Rosenthal, Experiments in control of flexible structure with non-collocated sensors and actuators, *Journal of Guidance Control and Dynamics*, 7 (5) (1984) 546-553.

[6] Q. Zhang, S. Shelley and R. J. Allemang, Active damping design of flexible structures based on SISO and SIMO non-collocated sensor-actuator velocity feedback, *Journal of Dynamic Systems, Measurement, and Control*, 113 (2) (1991) 259-266.

[7] G. Gatti, M. J. Brennan and P. Gardonio, Active damping of a beam using a piezoelectronic patch actuator, *Journal of Sound and Vibration*, 303 (2007) 798-813.

[8] C. Hong, Active control of resiliently-mounted flexible structures, Ph.D Thesis, Institute of sound and vibration research, University of Southampton.

[9] P. Gardonio, E. Bianchi and S. J. Elliot, Smart panel with multiple decentralized units for the control of sound transmission. Part II: design of the decentralized control units, *Journal of Sound and Vibration*, 274 (2004) 193-213.

[10] C. Hong and S. J. Elliott, Local feedback control of light honeycomb panels, *Journal of Acoustical Society of America*, 121 (1) (2007) 222-233.

[11] C. Hong, P. Gardonio and S. J. Elliott, Active control of resiliently mounted beams using triangular actuators, *Journal of Sound and Vibration*, 301 (2007) 297-318.

[12] J. L. Fanson and T. K. Caughey, Positive position feedback control for large space structures, *American Institue of Aeronautics and Astronautics*, 28 (4) (1990) 717-724.

[13] C. J. Goh and T. K. Caughey, On the stability problem caused by finte actuator dynamics in the collocated control of large space structures, *International Journal of Control*, 41 (3) (1985) 797-802.

[14] G. Song, S. P. Schmidt and B. N. Agrawal, Experimental robustness study of positive position feedback control for active vibration suppression, *Journal of Guidance Control and Dynamics*, 25 (1) (2002) 179-182.

[15] M. I. Friswell and D. J. Inman, The relationship between positive position feedback and output feedback controllers, *Smart Materials and Structures*, 8 (1999) 285-291.

[16] M. K. Kwak and S. Heo, Active vibration control of smart grid structure by multiinput and multioutput positive position feedback controller, *Journal of Sound and Vibration*, 304 (2007) 230-245.

[17] Z. Qiu, X. Zhang, H. Wu and H. Zhang, Optimal placement and active vibration control for piezoelectric smart flexible cantilever plate, *Journal of Sound and Vibration*, 301 (2007) 521-543.

[18] L. Meirovitch, *Analysis methods in vibration*, The Macmillan Company (1967).

[19] C. Hong and S. J. Elliot, Active control of resiliently-mounted beams with a moment pair actuator, *Smart Materials and Structures*, 14 (2005) 727-738.

[20] M. K. Kwak, S. Han and S. Heo, The stability conditions, performance and design methodology for the positive position feedback controller, *Transaction of the Korean Society for Noise and Vibration Engineering*, 14 (3) (2004) 208-213.

[21] C. M. Harris and A. G. Piersol, Harris' shock and vibraion handbook, McGraw-Hill (200).

Changjoo Shin received his B.S. Degree in 2006 from Pusan National University, Busan, South Korea, and is currently a Ph.D. candidate in School of Mechanical Engineering at Pusan National University.

Chinsuk Hong received his Ph.D. Degree from ISVR of University of Southampton in U.K., and is currently a Professor in School of Mechanical Engineering at Ulsan College in Ulsan, South Korea.

Weui Bong Jeong received his Ph.D. Degree from Tokyo Institute of Technology in Japan, and is currently a Professor in School of Mechanical Engineering at Pusan National University, Busan, South Korea.